Journal of Remote Sensing
A SCIENCE PARTNER JOURNAL
SPJ

Manuscript Template

FRONT MATTER

Title

Novel Use of Image Time-Series to Distinguish Dryland Vegetation Responses to Wet and Dry Years

Authors

Emily R. Myers[1,2*], Dawn M. Browning[1*], Laura M. Burkett[1], Darren K. James[1], Brandon T. Bestelmeyer[1]

1. USDA Agricultural Research Service, Jornada Experimental Range, Las Cruces, NM, US.
2. SCINet Program and ARS AI Center of Excellence, Office of National Programs, USDA Agricultural Research Service, Beltsville, MD 20705.

[*]Address correspondence to: Emily R. Myers; emily.r.myers@usda.gov and Dawn M. Browning; dawn.browning@usda.gov

Abstract

Remote sensing methods are commonly used to assess and monitor ecosystem conditions in drylands, but accurate classification and detection of ecological state change is challenging due to sparse vegetation cover, high spatial heterogeneity, and high inter-annual variability in production. We evaluated whether phenological metrics are effective for distinguishing ecological states using imagery from near-surface camera (PhenoCam) and satellite (Harmonized Landsat 8 and Sentinel-2, hereafter HLS), and how effectiveness varied across wet and dry rainfall years. We analyzed time series over 92 site-years at a desert grassland site in southwest New Mexico. Rainfall was a driver of phenological response across all ecological states, with wet years correlating with later start of season, later peak, higher peak greenness, and shorter growing season. This rainfall response was strongest in sandy shrub-invaded grasslands. PhenoCam estimated significantly earlier start of season than HLS for gravelly shrubland states, and earlier end of season than HLS for sandy shrub-invaded grassland states. We propose integrating seasonal metrics from high-frequency PhenoCam time series with satellite assessments to exploit phenological differences across variable rainfall years, improve monitoring efforts in drylands, and capture the timing and strength of peak greenness for grass-dominated ecological states as an indicator of ecological state change.

MAIN TEXT

1. Introduction

Drylands, which are estimated to cover over 40% of Earth's land surface [1], are ecologically important as they provide habitat to many native organisms, support crop production, serve as forage for livestock and wildlife, and contribute significantly to global atmospheric carbon dioxide (CO_2) regulation [2, 3]. Because of their low-fertility soil, unpredictable rainfall, and history of unsustainable land use, dryland ecosystems are highly susceptible to ecological state change [4]. Particularly concerning are shifts towards less biologically productive ecological states due to climate change and land use [4, 5, 6]. Ecological state-and-transition models (STM) provide a framework that helps landowners and managers identify ecologically vulnerable locations and manage them in a way designed to mitigate or even reverse degradation [7, 8, 9]. The foundation of an STM is spatially-explicit information based on composite soil, landscape position, and annual rainfall that designate the ecological site. Ecological site and state concepts are hierarchical, where ecological sites are defined by the static components of soil properties, landform, and climate, while ecological states represent the dynamic components of vegetation composition and diversity within a given ecological site.

An ecological state change of primary concern is the shift from perennial grasslands to shrublands [10, 11]. This state change has implications for CO_2 uptake and carbon storage in biomass and soil in widespread rangeland ecosystems due to differences in physiognomy, rooting depth and structure, phenology, and soil erosion potential [12, 13]. Grass species phenology and productivity have been shown to be more sensitive to rainfall than co-existing deeper-rooted shrub species [14, 15, 16, 17]. The degree to which species-level responses are observable via composite spectral responses depicted via satellite remote sensing (land surface phenology) is still debated [18].

Remote sensing data collected using sensor platforms ranging from near-surface cameras to airborne and satellite systems with repeated observations are essential for monitoring land surface condition [19] as well as estimating primary production [20]. Evaluations of ecological state change via remote sensing methods lag behind those for conservation and land use change (see [21]). Integrating data across remote sensing platforms is essential to capture ecological form and function in highly heterogeneous and variable dryland ecosystems [22]. Ground- or field-based data and perspectives provide a critical link between remote sensing and assessments of state change that can support the judicious use of resources to implement practices to mitigate or slow processes causing ecological state change [23].

Most remote sensing applications in drylands involve moderate to coarse resolution satellite image time series such as MODIS, Landsat, and Sentinel-2, and the harmonized Landsat 8 and Sentinel-2 (HLS) data product. Applications include mapping fractional cover [24, 25, 26, 27], ecological sites using hyper-temporal satellite time series [28], rangeland condition [19], land surface phenology monitoring and biomass [29, 30]. Studies combining daily, near-surface camera imagery (hereafter, 'PhenoCam') with 16-day satellite remote sensing imagery in drylands demonstrate the need for assessing metrics at multiple intervals in space and time [31, 32]. Due to differences in spatial and temporal resolution, satellite remotely sensed estimates of phenology do not always agree with near-surface measurements [32, 33, 34]. Disagreements between near-surface and satellite measurements may be exacerbated by issues of low vegetation cover, species composition (e.g., grass versus shrub) and high spatial and temporal variability in arid environments [3], as satellite measurements do not consistently detect green-up onset at low percentages of fractional cover [18].

Near-surface remote sensing data that have been available for dryland locations in the southwestern U.S. since 2014 have been used to quantify species and land surface phenology [15, 17, 32]. Data derived from PhenoCam time series images on the PhenoCam Network are more finely resolved than 30-m pixels in HLS time series, depict daily patterns in vegetation greenness, and are available on every continent [35]. Near-surface PhenoCam time series can potentially fill gaps in less-frequent, moderate resolution satellite time series for phenology monitoring, albeit with a few limitations [15]. Phenological metrics from satellite remote sensing have been coupled with ground-based measurements in a New Mexico desert grassland to reveal species-specific patterns in correspondence [15, 32]. Browning et al. [15] found that PhenoCam estimates for start of season for *Bouteloua eriopoda*, a C_4 stoloniferous perennial grass, were not detected until grasses reached 25% foliar cover, which could occur up to 60 days after plants produced new green culms (stems and leaves). Conversely, PhenoCam estimates for start and end of season for *Prosopis glandulosa*, a C_3 deciduous shrub, were within 7 days of field-observed start of season denoting production of new leaves.

Precipitation is the primary driver of aboveground biomass and productivity in this water-limited ecosystem with multi-year dry and wet periods differentially affecting grass and shrub biomass [14]. High inter-annual variability in precipitation timing and amount negatively affects grassland productivity, thereby decreasing resilience of grass-dominated states, whereas shrub productivity may increase following grass loss [36]. In water-limited arid ecosystems, it is important to consider plant responses during both resource-rich wet periods and intervening resource-limited dry periods [37, 38]. Currier and Sala [17] experimentally manipulated rainfall variability and estimated start and end of season for *Bouteloua eriopoda* grass and *Prosopis glandulosa* shrub using near-surface remote sensing. While precipitation was the primary driver of grass green-up and senescence, shrub green-up and senescence were insensitive to precipitation. In an analysis of phenology data over 23-years at the same site, Browning et al. [16] observed shrub green-up in March in over 65% (or 59) site-years spanning 1993 and 2015. Conversely, grass green-up was bimodally distributed across months with drought years associated with later green-up for grasses. There may be insight from differential responses to drought between grass and shrub species.

This study aimed to explore whether the presence of herbaceous productivity exhibits distinguishing phenological characteristics that can serve to monitor ecosystem function and identify ecological state change in drylands. To achieve this goal, we used remotely sensed image time series data from PhenoCam and HLS to derive phenological metrics and examine differences in ecosystem response between grass- and shrub-dominated ecological states in an arid rangeland.

We aimed to answer the following questions:

1. Do different ecological states exhibit distinct patterns expressed through phenological metrics? Do phenological metrics differ as derived from PhenoCam and HLS time-series?
2. Do ecological states with herbaceous productivity (or grass-dominated ecological states) show unique phenological properties compared to shrub-dominated ecological states? If yes, are differences equally discernable across both image platforms - PhenoCam and HLS?

3. For each ecological state, does precipitation affect how these phenological patterns are expressed?

Based on previous research of shrub and grass phenology, we expected that shrub-dominated and grass-dominated state classes would exhibit differences in phenology, and that those differences would be discernible using PhenoCam GCC and HLS EVI [15]. With respect to rainfall, we expected that grassy or grass-dominated states would exhibit greater inter-annual variability in phenological metrics, with later green-up and lower EVI amplitude in drought years, while shrub-dominated states would exhibit more consistent phenological responses across wet and dry years [16, 17].

2. Materials and Methods

2.1 Study Design

This study considered 12 different locations in southern New Mexico, representing 4 different ecological state classes. We used near-surface camera imagery and satellite imagery to obtain vegetation greenness time-series at 12 sites across multiple years between 2014 and 2022. Based on these time-series data, we calculated phenological metrics for each site-year. We identified site-years as wet, dry, or average as described in Section 2.3. We used ANOVA models to test for differences in phenological response across ecological state, imaging sensor, and rainfall. Each of these data collection, processing, and analysis steps is discussed in more detail in the following sections.

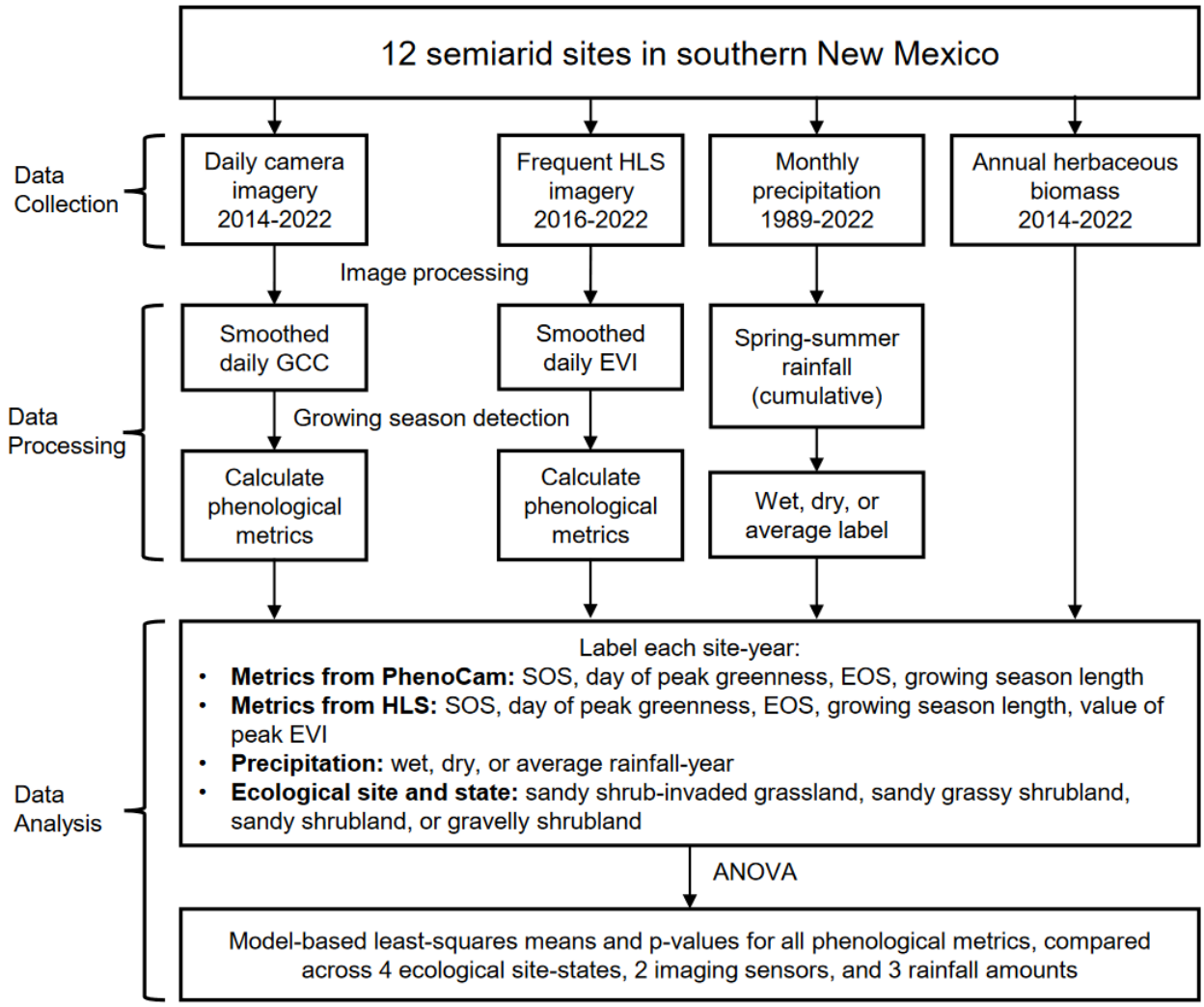

Fig. 1. Study design and analysis flowchart.

2.2 Study Site

This study was conducted on the Jornada Experimental Range (JER) in southern New Mexico, a 300 square mile outdoor laboratory established in 1912 and administered by the U.S. Department of Agriculture Agricultural Research Service [39]. This research focused on the twelve locations within the JER that contribute data to the PhenoCam network (Fig. 2). Long-term mean annual rainfall between 1915 and 1995 is 245.1 mm with 50% occurring during the months of July, August, and September. The mean air temperatures range between 3.8° C in January and 26.0° C in July [40].

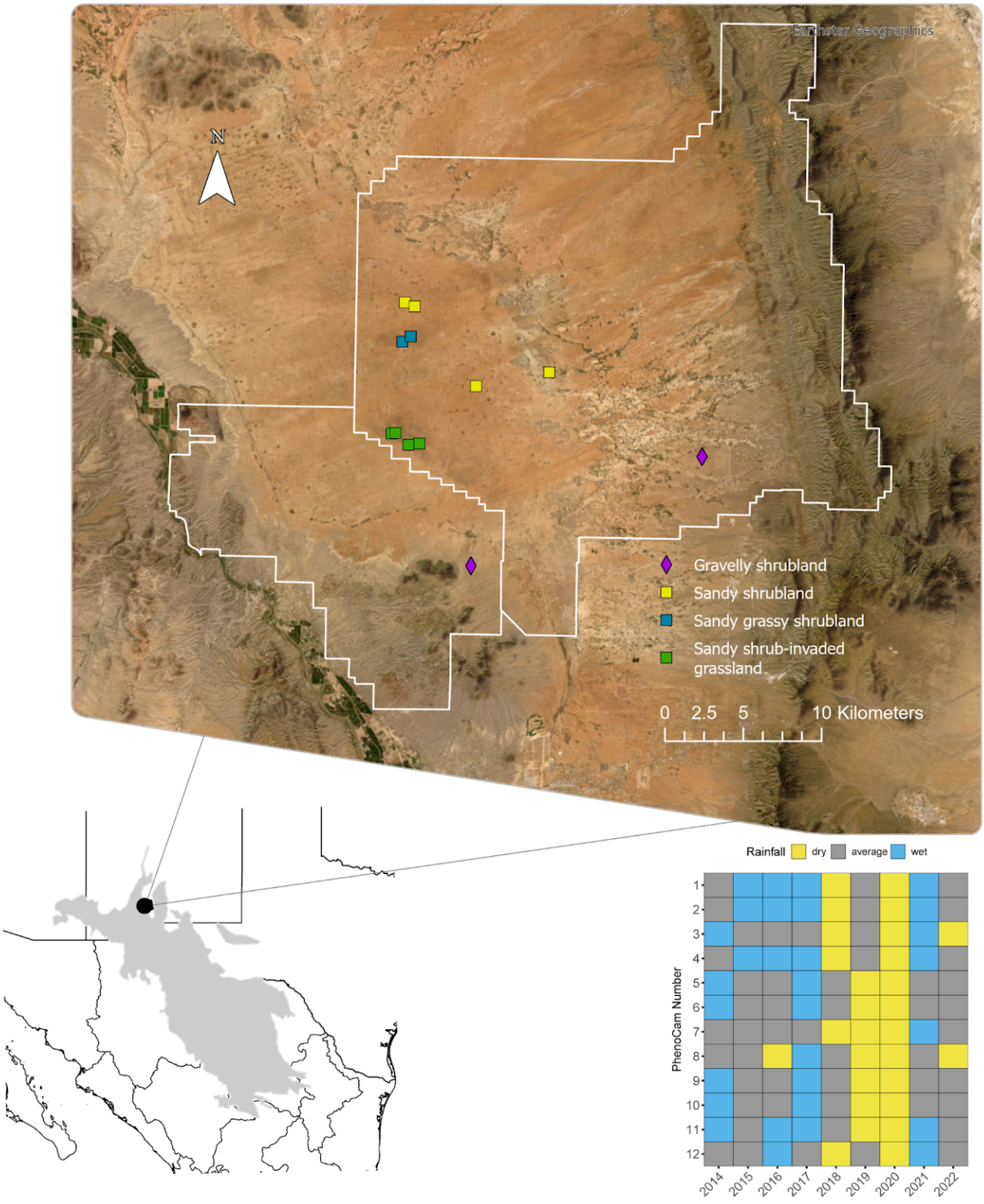

Fig 2. Map of twelve PhenoCam locations on the Jornada Experimental Range in southern New Mexico at the northern extent of the Chihuahuan Desert (gray outline) in inset image on bottom left. Grid on the bottom right shows wet, average, and dry year labels at PhenoCam sites from 2014-2022, based on total spring and summer precipitation (April 1 through September 30) across rain gauges in the JER.

Sandy soils in the study area are undergoing state change characterized by shrub encroachment into grasslands formerly dominated by *Bouteloua eriopoda* (black grama) with sub-dominant *Muhlenbergia porteri* (bush muhly) and *Sporobolus flexuosus* (mesa dropseed) perennial grass species. The deciduous shrub *Prosopis glandulosa* (honey mesquite) has increased in dominance on sandy soils, while, on gravelly soils, shrub encroachment is more advanced, leading to homogeneous shrublands dominated by the evergreen *Larrea tridentata* (creosote bush) [11, 41].

All ecological site and state classifications were determined using field-collected data. Within the twelve study sites, we considered four ecological state classes on two ecological sites that represent varying degrees of shrub encroachment with either honey mesquite or creosote bush present at all locations. This amounted to 12 PhenoCam locations across four ecological states, which included: deciduous shrub-invaded grassland on sandy soils (4 locations), grassy deciduous shrubland on sandy soils (2 locations), deciduous shrubland on sandy soils (4 locations), and evergreen shrubland on gravelly soils (2 locations). Grass-dominated states have more grass and less shrub biomass than shrub-dominated states with more exposed bare ground. See Table 1 and Fig. 3 for details and PhenoCam images for the study locations.

Table 1. PhenoCams on the Jornada Experimental Range (JER) in southern New Mexico used in this analysis through 2022. Ecosystem Dynamics Interpretive Tool (EDIT) code refers to ecological site descriptions for MLRA 42B (Southern Rio Grande Rift), LRU 42BB [42]. Links to associated ecological site descriptions are provided in Supp. Table S1.

Camera Number	PhenoCam Name	Ecological Site	EDIT Ecological Site Code	Ecological State	Dominant Species	Years of Data
1	ibp	Sandy	R042BB012NM	Shrub-invaded grassland	Black grama, honey mesquite	9
2	jergrassland	Sandy/ Shallow sandy	R042BB012NM/ R042BB015NM	Shrub-invaded grassland	Black grama, honey mesquite	3
3	jergrassland2	Sandy	R042BB012NM	Shrub-invaded grassland	Black grama, mesa dropseed, honey mesquite	1
4	NEON.D14.JORN.DP1.00033	Sandy	R042BB012NM	Shrub-invaded grassland/ grassland	Black grama, honey mesquite	5
5	jernovel	Sandy	R042BB012NM	Grassy shrubland	Honey mesquite, bush muhly	3
6	jernovel2	Sandy	R042BB012NM	Grassy shrubland	Honey mesquite,	1

					bush muhly	
7	jernort	Sandy	R042BB012NM	Shrubland	Honey mesquite	8
8	jernwern	Sandy/ Sandy loam	R042BB012NM/ N/A	Shrubland	Honey mesquite	5
9	jershrubland	Sandy	R042BB012NM	Shrubland	Honey mesquite	3
10	jershrubland2	Sandy	R042BB012NM	Shrubland	Honey mesquite	1
11	jerbajada	Gravelly	R042BB010NM	Shrubland	Creosote bush	8
12	jersand	Gravelly sand	R042BB024NM	Shrubland	Creosote bush	8

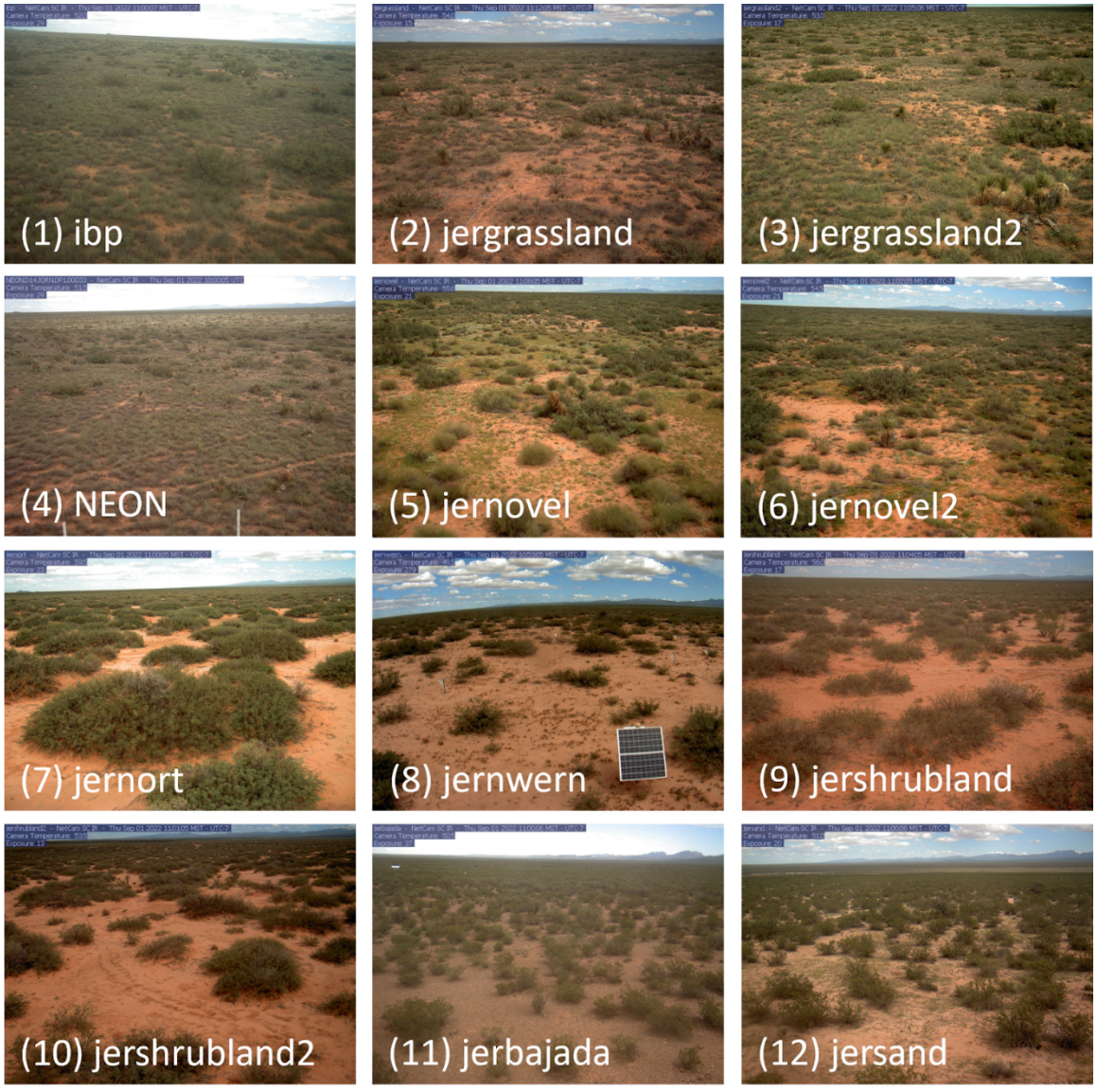

Fig. 3. PhenoCam images collected at twelve sites in the JER on 1 September 2022.

We used the primary site description for two sandy ecological sites with secondary ecological site descriptions (2 and 9 in Table 1). Locations identified as predominantly gravelly ecological sites (11 and 12) were also analyzed together as gravelly ecological sites. Direct links to the EDIT digital database for site descriptions can be found in Supp. Table S1.

2.3 Precipitation

To consider precipitation as a factor in our analysis, we evaluated greenness responses from two platforms across four ecological state classes for wet, dry, and average years between 2014 and 2022. The long-term mean (1989 - 2022) annual rainfall across selected rain gauges in the JER is 253 ± 74 mm, as calculated by monthly precipitation measurements from standard rain gauges located near PhenoCam sites [43, 44].

We examined seasons of precipitation to identify the best precipitation measure to use to model the phenological metrics from PhenoCam and HLS imagery (see next section); this analysis was done using R version 4.4.1 [45, 46]. Four seasons of precipitation were considered: winter (January 1-March 30), spring (April 1-June 30), summer (July 1-September 30), and fall (October 1-December 31); as well as several combined seasons: winter-spring, spring-summer, summer-fall, and total annual rainfall. For each of the three responses (start of season, peak, and end of season) we used separate linear regression models to model the relationship with the eight candidate measures of precipitation. We assessed model fit with the second-order Akaike Information Criterion (AIC) [47] and considered models within 2 AICc units of each other to not perform significantly better. In addition to the eight regression models for each response, we also included a null model in each candidate model set to serve as a benchmark for assessing model fit. Total spring and summer precipitation was correlated with the greatest number of phenological metrics, and was used in this study as a measure of the wetness or dryness of each growing season.

Estimates of cumulative spring and summer precipitation at each of the sites were determined by summing the monthly precipitation from the nearest rain gauge for each site. In months where "trace" amounts of precipitation were recorded, a value of 5 mm was used for the calculation. Spring and summer precipitation were compared to the long-term mean. Each site-year was considered a dry year if the spring-summer rainfall was more than 0.5 standardized mean differences below the long-term mean, and a wet year if the spring-summer rainfall was more than 0.5 standardized mean differences above the long-term mean. All site-years within 0.5 above or below the long-term mean were considered average.

The long-term mean spring and summer rainfall, calculated across all sites from 1989-2022, was 171 ± 64 mm. There was considerable variability across rain gauges within and across years. 2020 was the only year for which all site-years were classified as dry, although most sites received low rainfall in years 2018 through 2020 (Fig. 2).

2.4 Remotely Sensed Annual Herbaceous Biomass

We obtained estimated annual herbaceous biomass data from version 3 of the Rangeland Analysis Platform (RAP; [24, 48, 49]). RAP uses Landsat normalized difference vegetation index (NDVI) to estimate annual net primary productivity of annual and perennial forbs and grasses to 30m pixels across the contiguous United States. To obtain

biomass estimates at our PhenoCam locations during our period of interest (2014-2024) we averaged RAP pixels whose centroid occurred within a 45m buffer surrounding each Phenocam location. We then used a linear model to assess the effects of precipitation (dry, average, or wet), ecological state, and their interaction on annual biomass.

2.5 Time-Series Data

This study considered both near-surface digital camera imagery obtained from the PhenoCam network [50], and harmonized Landsat 8 and Sentinel-2 (HLS) satellite imagery [51]. The collection and processing of these data are described in the sections below.

2.5.1 PhenoCam Data

PhenoCam data for the 12 locations were obtained from the PhenoCam Network 2.0 [50]. At each of the 12 locations, a networked digital camera (StarDot Netcam SC 1.3 4 MP [StarDot, Buena Park, California, USA]) mounted approximately 6 m above the ground at a view angle of 20 degrees from the horizontal collects red, green, and blue (RGB) images every 15 minutes between 10 AM and 4 PM local time. Cameras were established at different times between 2013 and 2022 (Table 1).

A region of interest (ROI) containing a significant portion of the landscape was defined for each study site. For every image, the average canopy greenness, as defined by the green chromatic coordinate (GCC), was calculated over all of the pixels contained within the landscape-level ROI. GCC is given by the following equation:

$$GCC = G/(R + G + B) \quad (1)$$

where R, G, and B are the average green, red, and blue reflectance values recorded by the camera [52]. Because the PhenoCams do not collect near-infrared (NIR) information, commonly-used vegetation indices like the Normalized Difference Vegetation Index (NDVI) and Enhanced Vegetation Index (EVI) cannot be calculated from these data. From the raw GCC values, the 90th percentile of the GCC was calculated over a 3-day moving window, as shown in Fig. 6 of [52]. Using the 90th percentile of GCC and smoothing to a 3-day window helps reduce random noise in the GCC time-series that can occur due to variation in illumination conditions [50]. To obtain the final time-series data used in the analysis, the phenocamr R package was used to generate daily, smoothed GCC from the 3-day data. This package uses an iterative method to detect and filter out spurious GCC values due to bright events like rain or snow, and an AIC-based methodology to find and the optimal locally estimated scatterplot smoothing (LOESS) window [53].

For each site-year, growing seasons and their associated phenological metrics were identified using a modified version of the algorithm used by Bolton et al. to detect land surface phenology from harmonized Landsat 8 and Sentinel-2 (HLS) imagery [54]. The search window for candidate growing seasons within a site-year was defined as the 24-month period centered around that calendar year. Candidate growing season peaks within the search window were identified using the findpeaks function of the pracma R package [55]. In an iterative process starting with the smallest peak and ending with the largest peak, candidate peaks were eliminated if they occurred within 30 days of a larger peak or if the difference between the peak GCC and the pre- or post-peak minimum GCC was less than 35% of the total variation in GCC over the 24-month search window. Once valid peaks were identified, the days of pre- and post-peak minimum GCC (within 1 year of the peak) were identified and used to estimate start and end of season dates. The start of season (SOS) was the first day of the year after the pre-peak minimum when GCC was greater than or equal to 25% of the difference between peak GCC and pre-peak minimum

GCC. The end of season (EOS) was the last day of the year prior to the post-peak minimum when GCC was greater than or equal to 25% of the difference between peak GCC and post-peak minimum GCC. Although this method is similar to the threshold method used in other studies to determine SOS and EOS [15, 33], it differs slightly in that it is able to identify site-years where no growing seasons or multiple growing seasons occurred. SOS, EOS, and day of year (DOY) of peak were recorded for each valid growing season identified in each site-year. Instances of no peak or multiple peaks within a site-year were also recorded. For PhenoCam GCC, there were three site-years with no growing season: cameras 1 and 4 in 2018, and camera 2 in 2022. There were six site-years with two growing seasons: camera 5 in 2019, camera 4 in 2020, camera 3 in 2022, and camera 12 in 2016, 2019, and 2020 (Supp. Fig. S1).

2.5.2 Harmonized Landsat 8 and Sentinel-2 Data

The Harmonized Landsat 8 and Sentinel-2 (HLS) project is a NASA-produced data product consisting of 30 m multispectral surface reflectance every 2-3 days. Images from the Landsat 8 Operational Land Imager (OLI) are resampled into the 30 m Sentinel-2 tiling system and images from the Sentinel-2 Multispectral Instrument (MSI) are sampled into the 30 m Sentinel-2 tiling system and adjusted to the Landsat 8 spectral response function to create a combined image time-series that draws from Landsat 8, Sentinel-2A, and Sentinel-2B [54]. The HLS v2.0 L30 and S30 data products [56, 57], available over the study site from 2016-2022, were used for this analysis.

All HLS images for the 13SCS tile were downloaded and used to construct individual site time-series consisting of the 9-pixel square centered on each PhenoCam. Time-series data were cleaned using the Quality Assessment (QA) layer; pixels containing high aerosols, cloud, cloud shadow, or adjacent cloud were removed from the time-series. Enhanced Vegetation Index (EVI) values for each site were calculated using the cleaned data by averaging the 9 EVI pixels to represent a measure of canopy greenness over time. The equation for EVI is given below:

$$EVI = 2.5 \times \frac{NIR - R}{NIR + 6R - 7.5B + 1} \quad (2)$$

where R, B, and NIR are the red, blue, and near-infrared reflectance values. Although GCC was also considered, EVI was chosen over GCC for a couple of reasons. First, vegetation indices like EVI [30], 2-band EVI (EVI2) [34, 54], and NDVI [15, 24, 27, 28, 29, 33] are commonly used in MODIS, Landsat, and HLS vegetation analyses, while indices like GCC are less commonly used. Even in comparisons between satellite and PhenoCam, it is typical for phenological metrics derived from satellite EVI, EVI2, or NDVI to be compared with phenological metrics derived from PhenoCam GCC [15, 32, 33, 34]. Second, HLS-derived EVI values showed the greatest dynamic range over the growing season, compared to NDVI or GCC.

To obtain the final time-series data used in the analysis, locally estimated scatterplot smoothing (LOESS) with a span of 0.03 was used to estimate daily, smoothed EVI from the cleaned data. SOS, day of peak EVI, and EOS for all site-years were estimated using the same methods used for the PhenoCam data. In addition to these metrics, the value of peak EVI was recorded for each growing season. As with PhenoCam, instances of no peak within a site-year were recorded. For HLS EVI, there were eight site-years with no growing season: cameras 10 and 11 in 2016, cameras 1-4 in 2018, and cameras 2 and 3 in 2022. There were no site-years with multiple growing seasons recorded.

2.6 Statistical Analysis

We used ANOVA models to test for differences in four phenological responses: SOS, EOS DOY of peak GCC or EVI, and growing season length (GSL) for PhenoCam and HLS data. For site-years where multiple growing seasons were identified, we used the earliest SOS, latest EOS, and greatest peak and reported these instances by ecological state. Due to sample size imbalance between the sensors we used separate linear models for each sensor-response combination. We modeled ecological state (3-4 levels, depending on the sensor), spring-summer rainfall (three levels), and their interaction as fixed effects and included a random effect for sensor when possible.

To assess differences between sensors we calculated the pairwise difference for each year the two sensors had in common, then used linear models to assess the effects of ecological state, rainfall, and their interaction on these differences. We used the emmeans R packages [58] to calculate least squares means and compare them with the Sidak method. For all tests we used a significance level of 0.05.

3. Results

3.1 Remotely-Sensed Annual Herbaceous Biomass

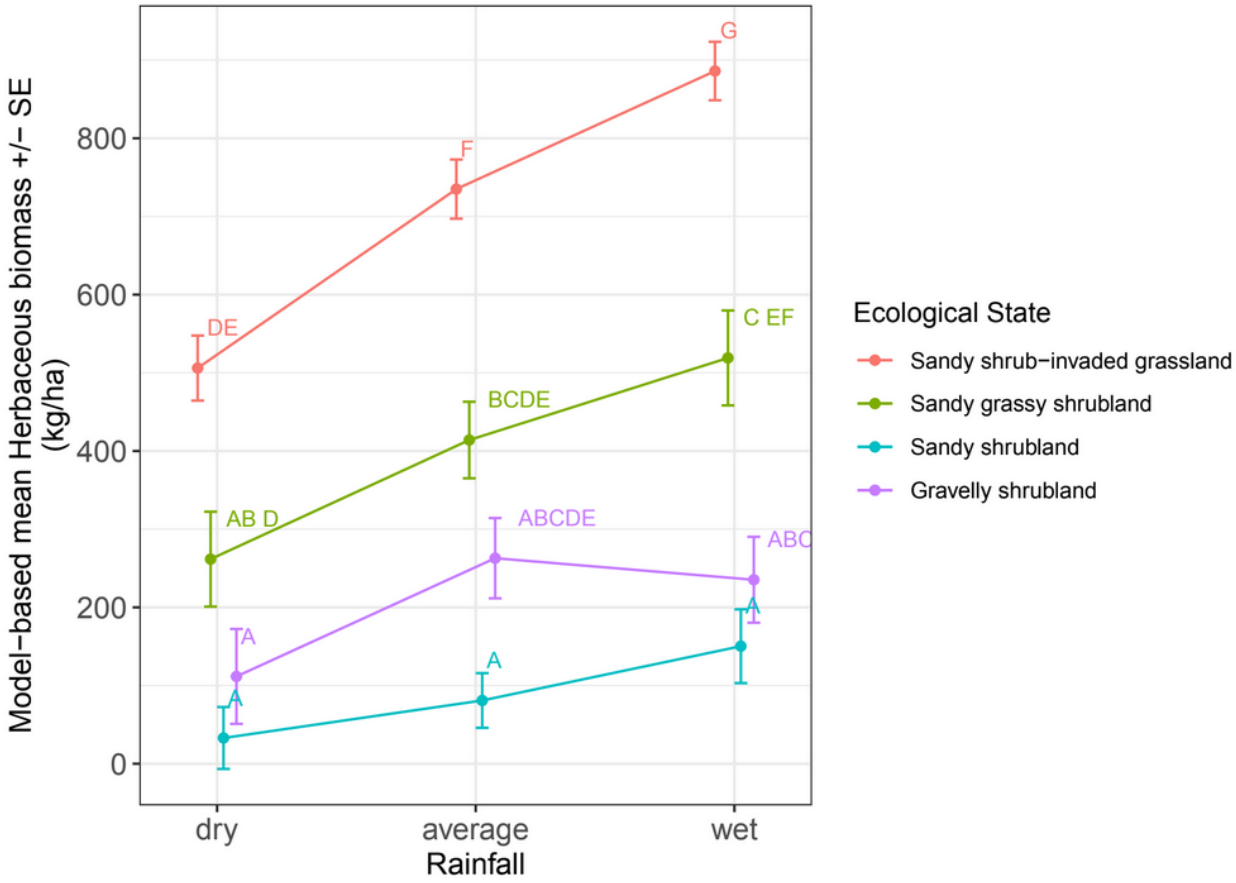

Fig. 4. Least-squares means and standard errors in model-based estimates of herbaceous biomass across different ecological states and rainfall amounts. Means with the same letter are not statistically different at $\alpha = 0.05$.

Herbaceous biomass increased with increasing grass cover and with increasing rainfall (Fig. 4). After accounting for rainfall, estimates of herbaceous biomass by state were 709 ± 32 kg/ha for sandy shrub-invaded grassland, 398 ± 46 kg/ha for sandy grassy shrubland, 88 ±

33 kg/ha for sandy shrubland, and 203 ± 45 kg/ha for gravelly shrubland. The sandy shrub-invaded grassland state, which has the highest percentage of grass cover, had a significantly higher annual herbaceous productivity than other ecological states. The sandy grassy shrubland state, which has the second highest percentage of grass cover, had a significantly higher annual herbaceous productivity than the sandy shrubland state. In addition, although herbaceous biomass at all states increased with increasing rainfall, sandy shrub-invaded grassland and sandy grassy shrubland showed the most significant differences in herbaceous biomass between wet and dry years.

3.2 Phenological Patterns Across Ecological States

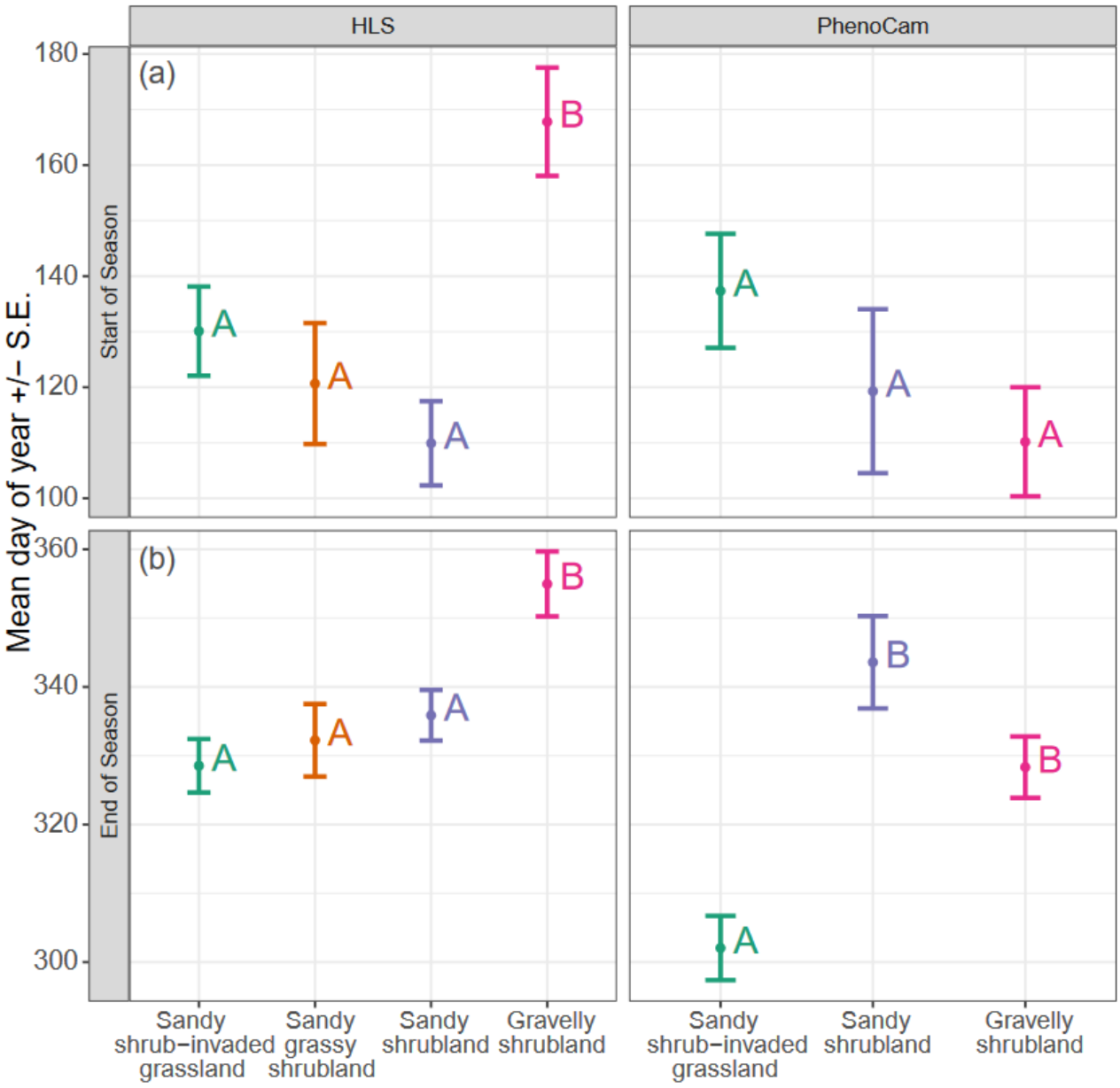

Fig. 5. Least-squares means and standard errors of model-based estimates of SOS and EOS across different ecological states for HLS (left) and PhenoCam (right). Within a plot, means with the same letter are not statistically different at α= 0.05.

With ecological state as a main effect, ANOVA models found that the most significant phenological differences across ecological states were in estimates of EOS (HLS: p =

0.0005; PhenoCam: $p < 0.0001$) and peak value of EVI ($p < 0.0001$). In addition, estimates of growing season length showed significant differences across ecological states (HLS: $p = 0.0397$; PhenoCam: $p = 0.0064$), likely driven by SOS (HLS only) and EOS (HLS and PhenoCam). Estimates of SOS showed significant differences across ecological states only for HLS data ($p = 0.0002$; Fig. 5a). In the HLS data, the gravelly shrubland state had a later EOS than other states. In the PhenoCam data, the sandy shrub-invaded grassland state had an earlier EOS than other states in non-dry years (Fig. 5b). Finally, in the HLS data, the gravelly shrubland state had a later start of season than other states (Fig. 5a). This differs from the PhenoCam data, in which all ecological states have a similar SOS. In general, there was a lot of overlap in phenological timings measured across different ecological states, as well as a high amount of variability within each state class. Some of this variability may be explained by other factors, such as rainfall.

3.3 Phenological Patterns Across Wet, Dry, Average Years

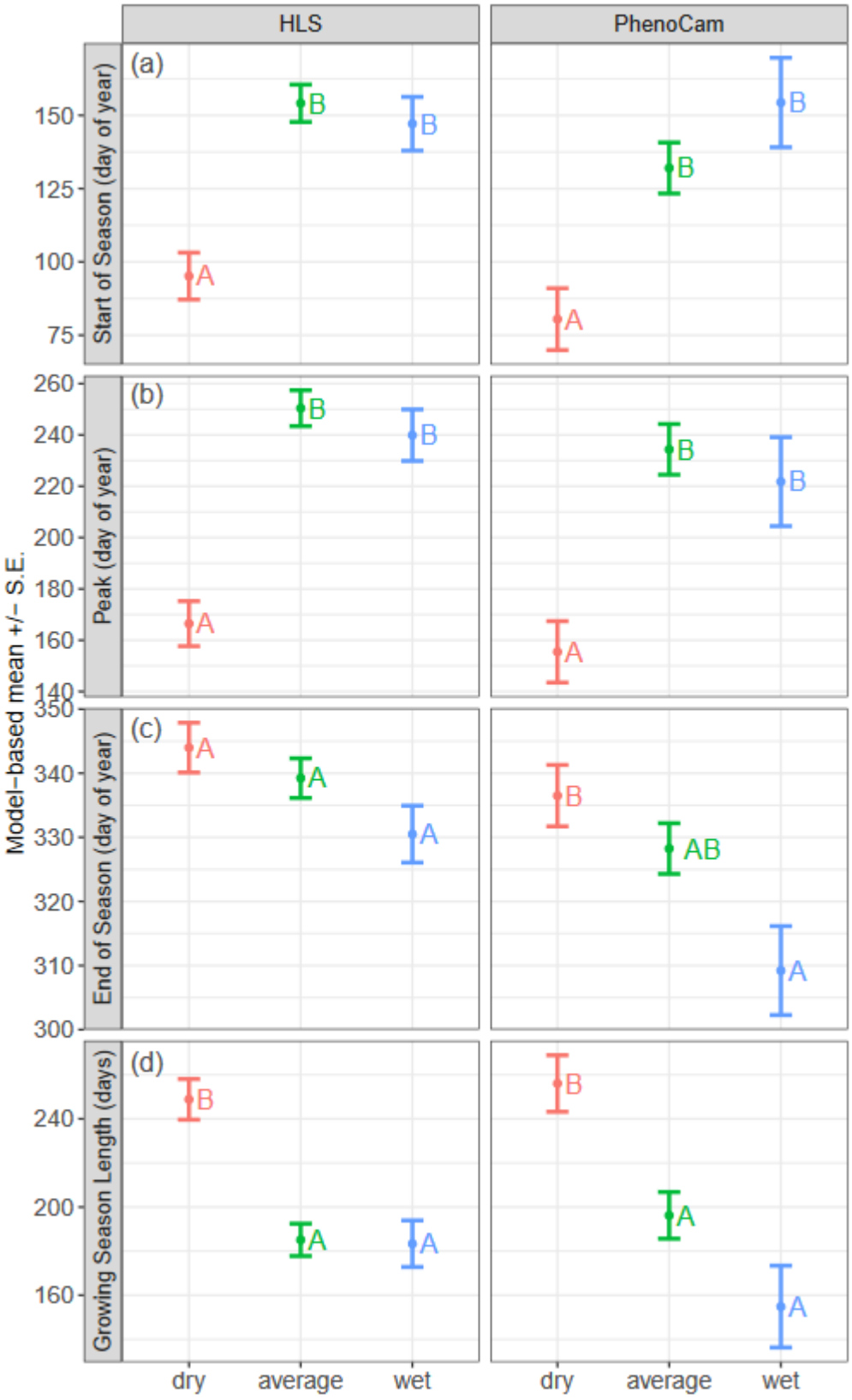

Fig. 6. Least-squares means and standard errors in model-based estimates of SOS, peak timing, EOS, and growing season length across different rainfall amounts for HLS (left) and PhenoCam (right). Within a panel, means with the same letter are not statistically different at α= 0.05.

With rainfall as a main effect, ANOVA models found significant differences across nearly all estimates of phenological metrics: SOS (HLS: $p < 0.0001$; PhenoCam: $p = 0.0002$; Fig. 6a), peak DOY (HLS: $p < 0.0001$; PhenoCam: $p = 0.0005$; Fig. 6b), EOS (PhenoCam: $p = 0.0102$; Fig. 6c), and growing season length (HLS: $p < 0.0001$; PhenoCam: $p < 0.0001$; Fig. 6d), and peak value of EVI ($p = 0.0014$).

Dry years led to earlier SOS, earlier peak, and longer growing season for all states except sandy grassy shrubland (Fig. 6). Wet years led to an earlier EOS across all states, although the differences between dry-year and wet-year EOS were only statistically significant for sandy shrub-invaded grassland. The peak value of EVI across all states increased with increasing spring-summer rainfall, which matches the trend in increasing herbaceous productivity (Fig. 4).

3.4 Phenological Patterns Across Rainfall and Ecological States

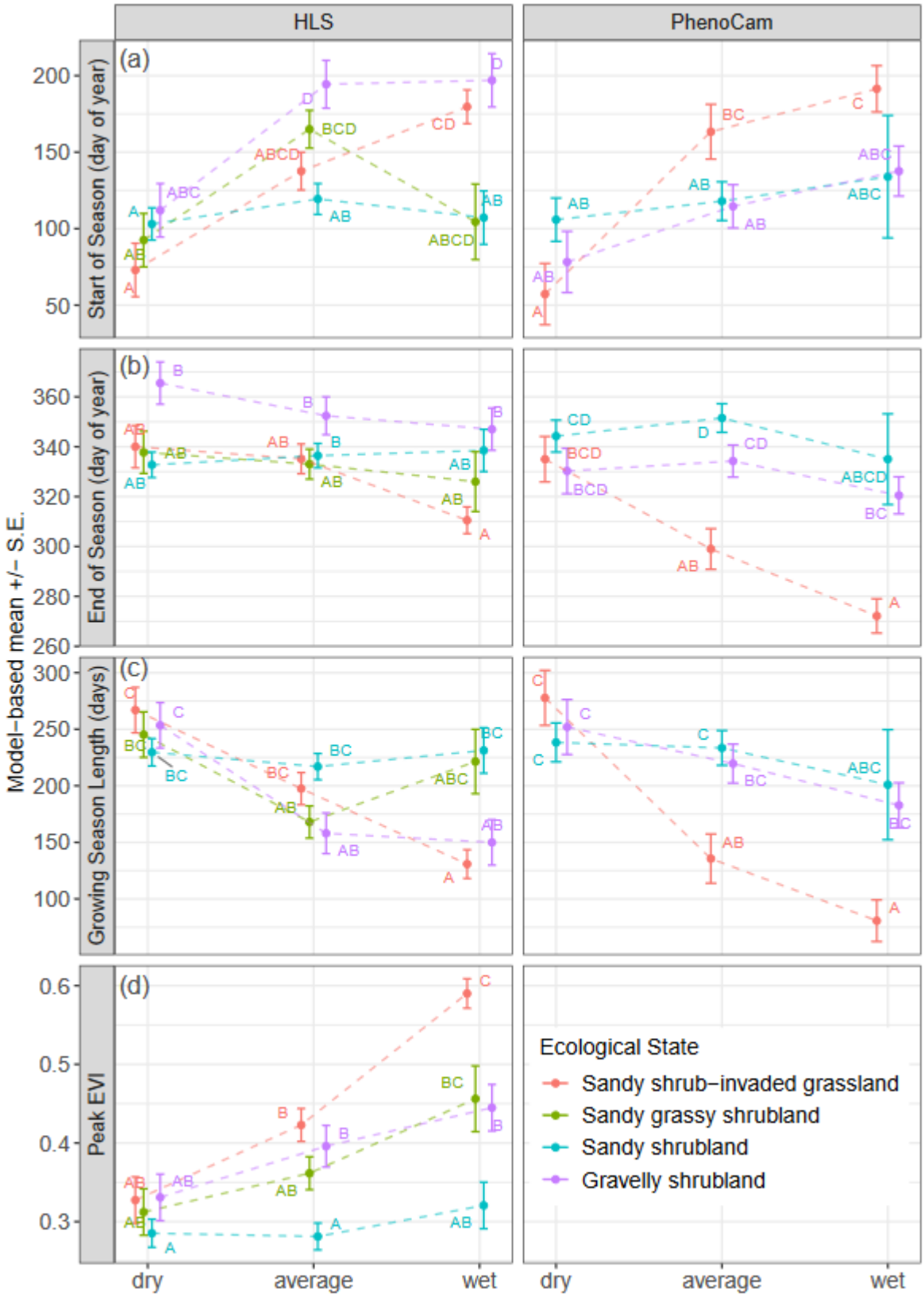

Fig. 7. Least-squares means and standard errors in model-based estimates of SOS, EOS, growing season length, and peak value of EVI across different ecological states and rainfall amounts for HLS (left) and PhenoCam (right). Within a panel, means with the same letter are not statistically different at $\alpha = 0.05$.

The sandy shrub-invaded grassland state was most affected by spring and summer rainfall, presumably attributed to herbaceous biomass that showed the highest value in wet years (Fig. 4). Sandy shrub-invaded grassland state demonstrated clear and distinct differences between wet and dry years for SOS (Fig. 7a), EOS (Fig. 7b), growing season length (Fig. 7c), and peak value of EVI (Fig. 7d).

The sandy shrub-invaded grassland state during dry or average rainfall years also comprised all but one of the site-years in which no growing season was detected. For the PhenoCam data, no growing season was detected in locations 1 and 4 in 2018 (dry year for both) and location 2 in 2022 (average precipitation, but significantly lower than the previous year). For the HLS data, no growing season was detected in locations 2 and 3 in 2018 (dry year for both) and 2022 (dry year for location 3, average precipitation for location 2, but significantly lower than the previous year), and location 10 in 2016 (average precipitation, but lower than surrounding years). Except for location 10, which is sandy shrubland, all site-years with no growing season were sandy shrub-invaded grassland states. Three of the six instances where two growing seasons were detected in PhenoCam data were also grass-dominated states in dry years: location 5 (sandy grassy shrubland) in 2019, location 4 (sandy shrub-invaded grassland) in 2020, and location 3 (sandy shrub-invaded grassland) in 2022.

3.5 Phenological Patterns Across Sensors

Estimates of SOS ($p = 0.0011$) and EOS ($p = 0.0091$) differed between HLS and PhenoCam across different ecological states. For gravelly shrubland states, HLS estimated a later SOS (168 ± 10) than PhenoCam (110 ± 10), particularly in non-dry years (Fig. 6). PhenoCam and HLS estimates of EOS also differed slightly across different states; sandy shrubland sites had an earlier EOS for HLS (336 ± 4) than for PhenoCam (342 ± 7), while sandy shrub-invaded grassland and gravelly shrubland sites usually had a later HLS-estimated EOS (sandy shrub-invaded grassland: 329 ± 4; gravelly shrubland: 355 ± 5) compared to PhenoCam (sandy shrub-invaded grassland: 304 ± 4; gravelly shrubland: 329 ± 4).

Comparisons between several of the gravelly shrubland site-years are shown in Supp. Fig. S2. For gravelly shrubland states, the PhenoCam data show small early-season bumps in GCC that are less pronounced in the HLS EVI for these sites. These differences in relative peak magnitude may be due to differences between the spectral indices. GCC has a lower dynamic range compared to EVI; it tends to saturate at higher levels of canopy greenness, and also reaches its minimum value before vegetation has finished senescing [52]. The estimates of peak DOY also differed between HLS and PhenoCam for a number of sites. These differences can be explained by the phenological curves for these years (Supp Fig. S3); all had a long period of near-peak greenness.

4. Discussion

In this study, we evaluated the ability of two remotely sensed image time series to detect differences in ecosystem function between different ecological states in arid rangelands. We quantified differences between phenological metrics calculated from PhenoCam and HLS time-series across different states, focusing on whether grass-dominated states express phenological patterns differently from shrub-dominated states. We also examined how growing-season phenology for all states differed between wet and dry years.

The unique contributions of this work are multiple. First, this study has a greater geographic scope compared to previous studies doing similar work; while other researchers have used remotely sensed imagery to evaluate dryland phenology [15, 17], they considered plants

within a single location rather than at multiple locations. Second, this study considers phenological responses at the landscape level, rather than at the level of individual plants. Evaluating landscape responses at multiple locations allows for a stronger, more compelling comparison between PhenoCam- and satellite-derived time-series data, since most satellites are not able to resolve individual plants. Finally, this study considers a higher spatial and temporal resolution satellite image source - HLS. While an increasing number of studies are using HLS for broader-scale land-surface phenology monitoring [54] or even for rangeland-specific mapping and monitoring [27], most studies like this one that compare phenology across multiple sensors have used coarser spatial resolution or less frequent satellite imagery than that of HLS [31, 32].

4.1 Phenological Patterns Across Ecological States

Ecological site and state affected estimates of EOS timing and growing season length in both datasets, and SOS timing and peak value of EVI in HLS data. In most cases, sandy shrub-invaded grassland states were the most distinguishable from other ecological states.

For PhenoCam specifically, sandy shrub-invaded grassland states had an earlier end of season than sandy or gravelly shrubland states in non-drought years. Sandy shrub-invaded grassland states also had a shorter growing season in non-drought years, driven by the earlier end of season. This finding is consistent with prior research on the green-up response and growing season length of shrubs and grasses at the JER [17]. The creosote bush-dominated gravelly shrubland states (11 and 12 in Fig. 3) proved more difficult to distinguish from other states, as there was a large spread in start of season estimates from both sensors, as well as disagreement between PhenoCam and HLS on the mean SOS timing for these site-years. The difficulty in estimating phenological metrics for the gravelly shrubland states is attributed to the evergreen nature of creosote bush, which maintains a baseline level of greenness throughout the year and often displays subtle shifts in greenness in response to deep soil moisture [59].

From the HLS data, the peak value of EVI varied across ecological states. Sandy shrub-invaded grassland states exhibited a much higher value of EVI than either type of shrubland site during wet years (Fig. 7d), which is consistent with the higher ground cover percentage of grasses compared to shrubs (visible in Fig. 3) as well as the documented grass responsiveness to rainfall [17, 60]. Sandy shrubland states demonstrated the lowest peak values of EVI across all rainfall conditions.

4.2 Phenological Patterns Across Wet, Dry, Average Years

Combined spring and summer precipitation was strongly correlated with estimates of start of season, growing season length (driven by start of season), and peak timing for time-series data derived from both PhenoCam and HLS. Across nearly all states and both sensor types, SOS and peak DOY occurred later during wet years and earlier during dry years, and EOS occurred slightly earlier during wet years. Although an earlier start of season during dry years seems counter-intuitive, we attribute it to the method of calculating start of season based on a threshold of 25% of the peak value. Drier years tended to have smaller peaks in GCC or EVI relative to baseline values, meaning that the VI threshold required to reach 25% of the scaled maximum was lower in dry years than in wet years and therefore easy to reach with even small increases in greenness. Even after eliminating peaks below the minimum required magnitude, most study locations still showed significant year-to-year variation in peak greenness.

For HLS data, the peak value of EVI was higher on average in wet years than in dry years. This difference in peak EVI between wet and dry years was most significant in sandy shrub-invaded grassland states and second most significant in sandy grassy shrubland states, which corresponds with precipitation-driven increases in herbaceous biomass for these grass-dominated states.

While we found promising correlations between total spring-summer precipitation and phenology, we acknowledge limitations in our analysis that are common with studies of vegetation dynamics in water-limited systems. First, precipitation in this region is highly spatially heterogeneous, meaning that precipitation measured at a rain gauge over 2,000 m away from a PhenoCam may not be representative of the rainfall at that PhenoCam location. Second, our labels of wet, dry, and average depended only on spring and summer rainfall. While this decision was based on a statistical analysis that showed high correlation between spring-summer rainfall and multiple phenological metrics, precipitation events outside of the spring and summer months influence soil water recharge that can influence phenology more for deeper-rooted species such as shrubs. For example, winter precipitation was found to be correlated with shrub SOS and peak timing in this study, and has also been linked to grass green-up by other researchers [17]. Additionally, multiple studies suggest that soil moisture - which is influenced by precipitation seasonal timing and temperature (which both affect evaporation), and size of precipitation events (which determines depth of water penetration into the soil) - may be more important than total precipitation for influencing vegetation greenness and productivity [13, 59, 61, 62]. Given these complexities, it is likely that exploring the link between precipitation and phenology using a moderate- to fine-resolution gridded data product for precipitation might yield additional or more refined insights.

We also show that plant communities can exhibit multiple greening and browning cycles in a year. Precipitation responses likely contributed to the multimodality in the phenology, which were particularly visible in grass-dominated (i.e., sandy shrub-invaded grassland, sandy grassy shrubland) states during dry years (e.g. Supp. Figure S1). Grass-dominated ecological states were also clearly conspicuous, with rapid increases in greenness in wet years (see Fig. 7c and 7d).

4.3 Ecological State Interactions with Rainfall and Sensor

4.3.1 Sandy Shrub-Invaded Grassland

Sandy shrub-invaded grassland states appeared to respond most strongly to spring-summer rainfall, with differences of 134.7 ± 24.9 days (PhenoCam) or 106.7 ± 20.7 days (HLS) between mean SOS estimates for wet and dry years, differences of 58.2 ± 11.8 days (PhenoCam) or 29.5 ± 10.0 days (HLS) between mean EOS estimates for wet and dry years, and differences of 193.0 ± 30.1 days (PhenoCam) or 136.2 ± 23.8 days (HLS) between mean growing season length estimates for wet and dry years. These differences are greater than for any other ecological state (Fig. 7). This finding is consistent with our understanding that dryland grasses are more responsive to short-term changes in water availability than shrubs, due in part to differences in root structure [17, 63]. The effect of spring-summer rainfall on peak value of EVI was also most pronounced in sandy shrub-invaded grassland sites, with a mean peak value of 0.590 ± 0.0187 in wet years and a mean peak value of 0.327 ± 0.0295 in dry years. These statistics do not include dry years in which no growing season was detected, which comprised the majority of no-peak site-years and tended to have even lower peak EVI. This confirms prior work indicating that growing-season precipitation is more important to the photosynthetic activity of grasses than shrubs at arid sites [32]. The

dynamic nature and positive response to rainfall can be an effective indicator of herbaceous productivity, which is confirmed by the high RAP estimates of herbaceous biomass for sandy shrub-invaded grassland states (Fig. 4).

4.3.2 Sandy Grassy Shrubland

Due to a low sample size, sandy grassy shrubland states were only analyzed using HLS data. These states diverged slightly from other ecological states in terms of SOS, which was latest during average rainfall years (Fig. 7), and peak timing, which was similar across all rainfall years. Although these differences may be due to differences in ground cover and productivity, it is much more likely that these differences are due to a low sample size for this state, which consisted of two study sites with only two wet site-years during the period of HLS coverage. When looking at the herbaceous biomass estimates (Fig. 4), which cover two additional years and add two more wet site-years to the analysis, the sandy grassy shrubland state appears to be in line with other ecological state responses to rainfall. It is expected that with a greater number of site-years for this state, its responses to rainfall would fall somewhere between those of sandy shrub-invaded grassland and sandy shrubland, in line with the different amounts of grass cover for each of these ecological states.

4.3.3 Sandy Shrubland

In general, sandy shrubland states appeared to respond least strongly to spring-summer rainfall, with statistically insignificant differences between wet- and dry-year estimates of SOS, EOS, growing season length, and peak value of EVI. As discussed in Section 4.1.2, some of this may be due to the choice of spring and summer rainfall for the precipitation metric - rainfall during other times of the year, like winter, may be more influential for shrub phenology than for grass phenology [17]. However, some of this lack of response to spring and summer rainfall may be due to lower overall peak greenness and productivity in mesquite shrubland sites compared to grassier sites (Figs. 4 and 7).

4.3.4 Gravelly Shrubland

PhenoCam and HLS estimates of start of season diverged for gravelly shrubland states, with HLS estimating a later start of season than PhenoCam (Fig. 7). For these creosote bush-dominated gravelly shrubland sites, later satellite SOS may be due to a combination of factors. First, differences in spatial resolution between sensors - the 30-m HLS pixels contain more bare ground than the PhenoCam photos, leading to a higher spatial variability overall and a potentially less pure greenness signal [3]. Second, creosote bush is evergreen, exhibiting a baseline level of greenness throughout the year that makes growing season green-up events more difficult to detect [59]. Finally, there are differences between EVI and GCC. GCC tends to saturate at high values of canopy greenness [64], meaning that the smaller early-season peaks in greenness present in the gravelly shrubland time-series are more prominent relative to the larger later-season peaks for GCC, compared to EVI. Studies looking at GCC suggest that changes in GCC correspond to changes in canopy structure at the start and end of the growing season [65], and changes in leaf color and pigmentation when gaps in the canopy are unchanging [65, 66]. Meanwhile, EVI is sensitive to leaf structure and changes in leaf area index (LAI) [67, 68], which continues to increase until late spring for evergreen plants. Peak EVI and herbaceous productivity for gravelly shrubland states were greater than for sandy shrubland states, but less than for sandy shrub-invaded grassland.

4.4 Implications and Future Work

Wet years yielded significant differences in phenological response for all ecological states - with later SOS, later peak, higher peak value of EVI, and shorter growing season length. Sandy shrub-invaded grassland states with the highest amount of grass cover exhibited the greatest differences in peak EVI, SOS, and EOS between wet and dry years. We also found that rapid spikes and high peaks in image time series to be a reliable indicator of the presence of grass or herbaceous productivity, a pattern that was clearest in wet years (Fig. 7c and 7d). We propose that presence of spikes in productivity, high peak vegetation index values, and shorter growing seasons in wet years can be used to identify grass species presence in conjunction with other remote sensing data. Coupling these proposed indicators with field assessments can enhance capabilities to identify ecological state change and monitor ecosystem function (e.g., higher or lower productivity). The "high peak" property in greenness can potentially serve as an indicator of herbaceous productivity in the context of multiple years.

Due to differences in rainfall response between states, it is easiest to use phenological metrics to distinguish between grass-dominated (e.g., shrub-invaded grassland and sandy grassy shrubland) and shrub-dominated (e.g., shrubland) states during periods of above-average rainfall [32]. During periods of drought, however, using phenological metrics to distinguish between grass- and shrub-dominated states is more challenging due to the already low dynamic range in arid rangeland vegetation greenness. The high year-to-year variability and significant overlap between phenological metrics for different ecological states, especially during dry years, may make it difficult to discern ecological site and state based only on remotely sensed phenology [69, 70]. However, by comparing metrics across different sensors, or by looking at the same site over a period of multiple years, we can improve our ability to discern between ecological function and phenology at different locations.

In the future, we would like to refine the hypotheses and algorithms to capture and evaluate the higher level of dynamism in grass-dominated states, which would require longer time series and ideally involve additional sites. In order to evaluate time-series spikiness, we would consider additional phenological metrics, like slope of green-up and senescence, as well as cumulative or integrated measures of greenness. In addition, we plan to explore quantitative methods to characterize the shape of the phenological profiles and use those to discern between different ecological sites and states.

4.5 Conclusions

Global drylands are susceptible to ecological state change. With added pressure from climate, these vast and often remote dry landscapes require remote sensing methods to detect and ideally ameliorate abrupt state change. We examined the utility of greenness time series from PhenoCams and satellite to determine whether grass-dominated ecological states exhibited distinguishing phenological properties, and how phenological metrics differed across platforms and between wet, average, and dry rainfall years. There were three notable findings from this study. Metrics for start and end of season for evergreen shrubland states were difficult to estimate because their year-round greenness makes seasonal changes in photosynthetic activity difficult to discern relative to the baseline value. Patterns in phenological metrics from PhenoCam and HLS time series were similar with greater detail in PhenoCam time series. There were interactions between ecological states and rainfall years, indicating differential responses to rainfall variability. Deciduous mesquite shrublands on sandy soils were insensitive to rainfall amount. Grass-dominated ecological states exhibited the strongest phenological responses to wet rain

years via higher peak greenness, later start of season and shorter growing season. Rapid, high peaks in greenness were attributed to grass or herbaceous responses. These properties can be used as indicators of grass productivity and indicators of ecological state change in drylands.

Acknowledgments

General: We would like to thank Ruben Baca, Julia Olivarez, and Neeshia Macanowicz for site research and support, and Sander Denham for providing helpful editorial comments on a draft of this manuscript.

Author Contributions: E. Myers and D. Browning conceptualized the study. E. Myers performed the analysis with support by D. James. E. Myers and D. Browning wrote the manuscript. L. Burkett collected field data. All authors revised the manuscript.

Funding: This research was supported by appropriated funds to the United States Department of Agriculture (USDA) Agricultural Research Service (ARS) Jornada Experimental Range project 3050-11210-009-00D, the Jornada Basin Long-Term Ecological Research Program DEB-1832194, and is a contribution from the Long-Term Agroecosystem Research (LTAR) network. The authors acknowledge the USDA ARS Big Data Initiative and SCINet high performance computing resources (https://scinet.usda.gov) made available for conducting the research reported in this paper. We thank collaborators for their efforts in support of PhenoCam Network. The development of PhenoCam has been funded by the Northeastern States Research Cooperative, NSF's Macrosystems Biology program (awards EF-1065029 and EF-1702697), DOE's Regional and Global Climate Modeling program (award DE-SC0016011) and the LTAR network which is supported by the USDA-ARS (Cooperative agreement 59-3050-2-002). Emily Myers was supported by a postdoctoral fellowship funded by the USDA Agricultural Research Service's SCINet Program and AI Center of Excellence, ARS project numbers 0201-88888-003-000D and 0201-88888-002-000D, and administered by the Oak Ridge Institute for Science and Education (ORISE) through an interagency agreement between the U.S. Department of Energy (DOE) and the U.S. Department of Agriculture (USDA). ORISE is managed by ORAU under DOE contract number DE-SC0014664. All opinions expressed in this paper are the author's and do not necessarily reflect the policies and views of USDA, DOE, or ORAU/ORISE.

Competing Interests: The authors declare that there is no conflict of interest regarding the publication of this article.

Data Availability: PhenoCam, HLS v2.0, and precipitation data are all publicly available, with sources cited in this submission. Novel code and derived data products are provided in the following repository: https://figshare.com/s/93e0cea081ea32a98409.

References

[1] Millennium Ecosystem Assessment. 2005. "Ecosystems and Human Well-being: Desertification Synthesis." World Resources Institute, Washington, DC.

[2] Ahlstrom, A., M. R. Raupach, G. Schurgers, B. Smith, A. Arneth, M. Jung, M. Reichstein, J. G. Canadell, P. Friedlingstein, A. K. Jain, E. Kato, B. Poulter, S. Sitch, B. D. Stocker, N.

Viovy, Y. P. Wang, A. Wiltshire, S. Zaehle, and N. Zeng. 2015. "The dominant role of semi-arid ecosystems in the trend and variability of the land CO2 sink." Science 348 (6237):895-899. doi: 10.1126/science.aaa1668.

[3] Smith, William K., Matthew P. Dannenberg, Dong Yan, Stefanie Herrmann, Mallory L. Barnes, Greg A. Barron-Gafford, Joel A. Biederman, et al. 2019. "Remote Sensing of Dryland Ecosystem Structure and Function: Progress, Challenges, and Opportunities." Remote Sensing of Environment 233 (November): 111401. https://doi.org/10.1016/j.rse.2019.111401.

[4] Bestelmeyer, Brandon T, Gregory S Okin, Michael C Duniway, Steven R Archer, Nathan F Sayre, Jebediah C Williamson, and Jeffrey E Herrick. 2015. "Desertification, Land Use, and the Transformation of Global Drylands." Frontiers in Ecology and the Environment 13 (1): 28–36. https://doi.org/10.1890/140162.

[5] Peters, Debra P. C., Jin Yao, Osvaldo E. Sala, and John P. Anderson. 2012. "Directional Climate Change and Potential Reversal of Desertification in Arid and Semiarid Ecosystems." Global Change Biology 18 (1): 151–63. https://doi.org/10.1111/j.1365-2486.2011.02498.x.

[6] Peters, Debra P. C., and J Yao. 2012. "Long-Term Experimental Loss of Foundation Species: Consequences for Dynamics at Ecotones across Heterogeneous Landscapes." Ecosphere 3 (3): art27. https://doi.org/10.1890/ES11-00273.1.

[7] Brown, Joel R., and Kris M. Havstad. 2016. "Using Ecological Site Information to Improve Landscape Management for Ecosystem Services." Rangelands 38 (6): 318–21. https://doi.org/10.1016/j.rala.2016.10.011.

[8] Duniway, Michael C., Christopher Benson, Travis W. Nauman, Anna Knight, John B. Bradford, Seth M. Munson, Dana Witwicki, et al. 2022. "Geologic, Geomorphic, and Edaphic Underpinnings of Dryland Ecosystems: Colorado Plateau Landscapes in a Changing World." Ecosphere 13 (11): e4273. https://doi.org/10.1002/ecs2.4273.

[9] Briske, D.D., B.T. Bestelmeyer, T.K. Stringham, and P.L. Shaver. 2008. "Recommendations for Development of Resilience-Based State-and-Transition Models." Rangeland Ecology & Management 61 (4): 359–67. https://doi.org/10.2111/07-051.1.

[10] Eldridge, David J., Matthew A. Bowker, Fernando T. Maestre, Erin Roger, James F. Reynolds, and Walter G. Whitford. 2011. "Impacts of shrub encroachment on ecosystem structure and functioning: towards a global synthesis." Ecology Letters 14:709-722. doi: 10.1111/j.1461-0248.2011.01630.x.

[11] Bestelmeyer, Brandon T, Debra P C Peters, Steven R Archer, Dawn M Browning, Gregory S Okin, Robert L Schooley, and Nicholas P Webb. 2018. "The Grassland–Shrubland Regime Shift in the Southwestern United States: Misconceptions and Their Implications for Management." BioScience 68 (9): 678–90. https://doi.org/10.1093/biosci/biy065.

[12] Petrie, M. D., S. L. Collins, A. M. Swann, P. L. Ford, and M.E. Litvak. 2015. "Grassland to Shrubland State Transitions Enhance Carbon Sequestration in the Northern Chihuahuan Desert." Global Change Biology 21 (3): 1226–35. https://doi.org/10.1111/gcb.12743.

[13] Collins, S.L., J. Belnap, N.B. Grimm, J.A. Rudgers, C.N. Dahm, P. D'Odorico, M. Litvak, et al. 2014. "A Multiscale, Hierarchical Model of Pulse Dynamics in Arid-Land Ecosystems." Annual Review of Ecology, Evolution, and Systematics 45 (1): 397–419. https://doi.org/10.1146/annurev-ecolsys-120213-091650.

[14] Peters, D. C., Jin Yao, Dawn M. Browning, and Albert Rango. 2014. "Mechanisms of grass response in grasslands and shrublands during dry or wet periods." Oecologia 174:1323-1334. doi: 10.1007/s00442-013-2837-y.

[15] Browning, Dawn, Jason Karl, David Morin, Andrew Richardson, and Craig Tweedie. 2017. "Phenocams Bridge the Gap between Field and Satellite Observations in an Arid Grassland Ecosystem." Remote Sensing 9 (10): 1071. https://doi.org/10.3390/rs9101071.

[16] Browning, D.M., Crimmins Theresa M., Darren K. James, Sheri Spiegal, Matthew R. Levi, John P. Anderson, and Debra C. Peters. 2018. "Synchronous species responses identify phenological guilds – Implications for management." Ecosphere 9 (9):e02395. doi: 10.1002/ecs2.2395.

[17] Currier, Courtney M., and Osvaldo E. Sala. 2022. "Precipitation versus Temperature as Phenology Controls in Drylands." Ecology 103 (11). https://doi.org/10.1002/ecy.3793.

[18] Taylor, Shawn D., Dawn M. Browning, Ruben A. Baca, and Feng Gao. 2021. "Constraints and Opportunities for Detecting Land Surface Phenology in Drylands." Journal of Remote Sensing 2021 (January): 2021/9859103. https://doi.org/10.34133/2021/9859103.

[19] Retallack, A., G. Finlayson, B. Ostendorf, K. Clarke, and M. Lewis. 2023. "Remote sensing for monitoring rangeland condition: Current status and development of methods." Environmental and Sustainability Indicators 19:18. doi: 10.1016/j.indic.2023.100285.

[20] Running, S. W., R. R. Nemani, F. A. Heinsch, M. S. Zhao, M. Reeves, and H. Hashimoto. 2004. "A continuous satellite-derived measure of global terrestrial primary production." Bioscience 54 (6):547-560.

[21] Willis, K. S. 2015. "Remote sensing change detection for ecological monitoring in United States protected areas." Biological Conservation 182:233-242. doi: 10.1016/j.biocon.2014.12.006.

[22] Browning, D.M., A. Rango, J. W. Karl, C. M. Laney, E. R. Vivoni, and C. E. Tweedie. 2015. "Emerging technological and cultural shifts advancing drylands research and management." Frontiers in Ecology and the Environment 13 (1):52-60. doi: 10.1890/140161.

[23] Bestelmeyer, B., Sarah McCord, Dawn Browning, Laura Burkett, Emile Elias, Rick Estell, Jeffrey Herrick, Darren James, Sheri Spiegal, Santiago Utsumi, Nicholas Webb, and Jeb Williamson. 2024. "Fulfilling the promise of digital tools to build rangeland resilience." Frontiers in Ecology and the Environment:32736. doi: https://doi.org/10.1002/fee.2736.

[24] Allred, Brady W., Brandon T. Bestelmeyer, Chad S. Boyd, Christopher Brown, Kirk W. Davies, Michael C. Duniway, Lisa M. Ellsworth, et al. 2021. "Improving Landsat Predictions of Rangeland Fractional Cover with Multitask Learning and Uncertainty." Edited by Robert

Freckleton. Methods in Ecology and Evolution 12 (5): 841–49. https://doi.org/10.1111/2041-210X.13564.

[25] Shi, Hua, Matthew Rigge, Kory Postma, and Brett Bunde. 2022. "Trends Analysis of Rangeland Condition Monitoring Assessment and Projection (RCMAP) Fractional Component Time Series (1985–2020)." GIScience & Remote Sensing 59 (1): 1243–65. https://doi.org/10.1080/15481603.2022.2104786.

[26] Rigge, Matthew, Collin Homer, Hua Shi, Debra Meyer, Brett Bunde, Brian Granneman, Kory Postma, Patrick Danielson, Adam Case, and George Xian. 2021. "Rangeland Fractional Components Across the Western United States from 1985 to 2018." Remote Sensing 13 (4): 813. https://doi.org/10.3390/rs13040813.

[27] Dahal, Devendra, Neal J. Pastick, Stephen P. Boyte, Sujan Parajuli, Michael J. Oimoen, and Logan J. Megard. 2022. "Multi-Species Inference of Exotic Annual and Native Perennial Grasses in Rangelands of the Western United States Using Harmonized Landsat and Sentinel-2 Data." Remote Sensing 14 (4): 807. https://doi.org/10.3390/rs14040807.

[28] Maynard, JJ, and JW Karl. 2017. "A Hyper-Temporal Remote Sensing Protocol for High-Resolution Mapping of Ecological Sites." PLOS ONE 12 (4). https://doi.org/10.1371/journal.pone.0175201.

[29] Kearney, Sean P., Lauren M. Porensky, David J. Augustine, Rowan Gaffney, and Justin D. Derner. 2022. "Monitoring Standing Herbaceous Biomass and Thresholds in Semiarid Rangelands from Harmonized Landsat 8 and Sentinel-2 Imagery to Support within-Season Adaptive Management." Remote Sensing of Environment 271 (March): 112907. https://doi.org/10.1016/j.rse.2022.112907.

[30] Xie, Qiaoyun, Jamie Cleverly, Caitlin E. Moore, Yanling Ding, Christopher C. Hall, Xuanlong Ma, Luke A. Brown, et al. 2022. "Land Surface Phenology Retrievals for Arid and Semi-Arid Ecosystems." ISPRS Journal of Photogrammetry and Remote Sensing 185 (March): 129–45. https://doi.org/10.1016/j.isprsjprs.2022.01.017.

[31] Yan, D, RL Scott, DJP Moore, JA Biederman, and WK Smith. 2019. "Understanding the Relationship between Vegetation Greenness and Productivity across Dryland Ecosystems through the Integration of PhenoCam, Satellite, and Eddy Covariance Data." REMOTE SENSING OF ENVIRONMENT 223 (March): 50–62. https://doi.org/10.1016/j.rse.2018.12.029.

[32] Morisette, Jeffrey T., Katharyn A. Duffy, Jake F. Weltzin, Dawn M. Browning, R. Lee Marsh, Aaron M. Friesz, Luke J. Zachmann, et al. 2021. "PS3: The Pheno-Synthesis Software Suite for Integration and Analysis of Multi-Scale, Multi-Platform Phenological Data." Ecological Informatics 65 (November): 101400. https://doi.org/10.1016/j.ecoinf.2021.101400.

[33] Browning, Dawn M., Eric S. Russell, Guillermo E. Ponce-Campos, Nicole Kaplan, Andrew D. Richardson, Bijan Seyednasrollah, Sheri Spiegal, et al. 2021. "Monitoring Agroecosystem Productivity and Phenology at a National Scale: A Metric Assessment Framework." Ecological Indicators 131 (November): 108147. https://doi.org/10.1016/j.ecolind.2021.108147.

[34] Donnelly, Alison, Rong Yu, Katherine Jones, Michael Belitz, Bonan Li, Katharyn Duffy, Xiaoyang Zhang, et al. 2022. “Exploring Discrepancies between in Situ Phenology and Remotely Derived Phenometrics at NEON Sites.” Ecosphere 13 (1). https://doi.org/10.1002/ecs2.3912.

[35] Richardson, A. D. 2023. "PhenoCam: An evolving, open-source tool to study the temporal and spatial variability of ecosystem-scale phenology." Agricultural and Forest Meteorology 342:18. doi: 10.1016/j.agrformet.2023.109751.

[36] Gherardi, Laureano A., and Osvaldo E. Sala. 2015. “Enhanced Precipitation Variability Decreases Grass- and Increases Shrub-Productivity.” *Proceedings of the National Academy of Sciences* 112 (41): 12735–40. https://doi.org/10.1073/pnas.1506433112.

[37] Post, A. K., and A. K. Knapp. 2020. "The importance of extreme rainfall events and their timing in a semi-arid grassland." Journal of Ecology 108 (6):2431-2443. doi: 10.1111/1365-2745.13478.

[38] Hoover, D. L., O. L. Hajek, M. D. Smith, K. Wilkins, I. J. Slette, and A. K. Knapp. 2022. "Compound hydroclimatic extremes in a semi-arid grassland: Drought, deluge, and the carbon cycle." Global Change Biology 28 (8):2611-2621. doi: 10.1111/gcb.16081.

[39] Havstad, K.M., W.P. Kustas, A. Rango, J.C. Ritchie, and T.J. Schmugge. 2000. “Jornada Experimental Range: A Unique Arid Land Location for Experiments to Validate Satellite Systems.” Remote Sensing of Environment 74 (1): 13–25. https://doi.org/10.1016/S0034-4257(00)00118-8.

[40] Wainwright, John. 2006. "Climate and Climatological Variations in the Jornada Basin." In Structure and Function of a Chihuahuan Desert Ecosystem. The Jornada Basin Long-Term Ecological Research Site, edited by Kris M. Havstad, Laura F. Huennecke and William H. Schlesinger, 44-80. Oxford, England: Oxford University Press.

[41] Archer, Steven R., Debra P. C. Peters, N. Dylan Burruss, and Jin Yao. 2022. “Mechanisms and Drivers of Alternative Shrubland States.” Ecosphere 13 (4). https://doi.org/10.1002/ecs2.3987.

[42] USDA Natural Resources Conservation Service, USDA Agricultural Research Service Jornada Experimental Range, and New Mexico State University. 2023.“Southern Rio Grande Rift.” Ecosystem Dynamics Interpretive Tool (EDIT). Accessed August 14, 2023. https://edit.jornada.nmsu.edu/catalogs/esd/042B.

[43] Thatcher, David, and Brandon T Bestelmeyer. 2023. “Monthly Precipitation Data from a Network of Standard Gauges at the Jornada Experimental Range (Jornada Basin LTER) in Southern New Mexico, January 1916 - Ongoing.” Environmental Data Initiative. https://doi.org/10.6073/PASTA/CAAE15334E7707AF04BB761C14079E57.

[44] Abrahams, Athol, Walter G Whitford, Laura F Huenneke, David C Lightfoot, John Anderson, Anthony Parsons, and John Wainwright. 2023. “Graduated Rain Gauge (GRG) Precipitation Observations from 21 Sites at the Jornada Basin LTER Site, 1989-Ongoing.” Environmental Data Initiative. https://doi.org/10.6073/PASTA/DD23997906FEAA5C5B6A29BE63300BFD.

[45] R Core Team. 2021. “R: A Language and Environment for Statistical Computing.” Vienna, Austria: R Foundation for Statistical Computing. https://www.R-project.org.

[46] Wickham, Hadley, Mara Averick, Jennifer Bryan, Winston Chang, Lucy McGowan, Romain François, Garrett Grolemund, et al. 2019. “Welcome to the Tidyverse.” Journal of Open Source Software 4 (43): 1686. https://doi.org/10.21105/joss.01686.

[47] Mazerolle, Marc J. 2023. “AICcmodavg: Model Selection and Multimodel Inference Based on (Q)AIC(c).” https://cran.r-project.org/package=AICcmodavg.

[48] Jones, M.O., N.P. Robinson, D.E. Naugle, J.D. Maestas, M.C. Reeves, R.W. Lankston, and B.W. Allred. 2021. Annual and 16-Day Rangeland Production Estimates for the Western United States. Rangeland Ecology & Management 77:112-117. http://dx.doi.org/10.1016/j.rama.2021.04.003

[49] Robinson, N. P., M. O. Jones, A. Moreno, T. A. Erickson, D. E. Naugle, and B. W. Allred. 2019. Rangeland productivity partitioned to sub-pixel plant functional types. Remote Sensing 11:1427. http://dx.doi.org/10.3390/rs11121427.

[50] Richardson, Andrew D., Koen Hufkens, Tom Milliman, Donald M. Aubrecht, Min Chen, Josh M. Gray, Miriam R. Johnston, et al. 2018. “Tracking Vegetation Phenology across Diverse North American Biomes Using PhenoCam Imagery.” Scientific Data 5 (1): 180028. https://doi.org/10.1038/sdata.2018.28.

[51] Claverie, Martin, Junchang Ju, Jeffrey G. Masek, Jennifer L. Dungan, Eric F. Vermote, Jean-Claude Roger, Sergii V. Skakun, and Christopher Justice. 2018. “The Harmonized Landsat and Sentinel-2 Surface Reflectance Data Set.” Remote Sensing of Environment 219 (December): 145–61. https://doi.org/10.1016/j.rse.2018.09.002.

[52] Sonnentag, O., K. Hufkens, C. Teshera-Sterne, A. M. Young, M. Friedl, B. H. Braswell, T. Milliman, J. O'Keefe, and A. D. Richardson. 2012. "Digital repeat photography for phenological research in forest ecosystems." Agricultural and Forest Meteorology 152:159-177. doi: 10.1016/j.agrformet.2011.09.009.

[53] Hufkens, Koen, David Basler, Tom Milliman, Eli K. Melaas, and Andrew D. Richardson. 2018. “An Integrated Phenology Modelling Framework in r.” Edited by Sarah Goslee. Methods in Ecology and Evolution 9 (5): 1276–85. https://doi.org/10.1111/2041-210X.12970.

[54] Bolton, Douglas K., Josh M. Gray, Eli K. Melaas, Minkyu Moon, Lars Eklundh, and Mark A. Friedl. 2020. “Continental-Scale Land Surface Phenology from Harmonized Landsat 8 and Sentinel-2 Imagery.” Remote Sensing of Environment 240 (April): 111685. https://doi.org/10.1016/j.rse.2020.111685.

[55] Borchers, Hans W. 2023. “pracma: Practical Numerical Math Functions.” https://cran.r-project.org/web/packages/pracma/.

[56] Masek, Jeffrey, Junchang Ju, Jean-Claude Roger, Sergii Skakun, Eric Vermote, Martin Claverie, Jennifer Dungan, Zhangshi Yin, Brian Freitag, and Chris Justice. 2021. “HLS Operational Land Imager Surface Reflectance and TOA Brightness Daily Global 30m v2.0.”

NASA EOSDIS Land Processes Distributed Active Archive Center. https://doi.org/10.5067/HLS/HLSL30.002.

[57] Masek, Jeffrey, Junchang Ju, Jean-Claude Roger, Sergii Skakun, Eric Vermote, Martin Claverie, Jennifer Dungan, Zhangshi Yin, Brian Freitag, and Chris Justice. 2021. "HLS Sentinel-2 Multi-Spectral Instrument Surface Reflectance Daily Global 30m v2.0." NASA EOSDIS Land Processes Distributed Active Archive Center. https://doi.org/10.5067/HLS/HLSS30.002.

[58] Lenth, Russell V. 2022. "Emmeans: Estimate MArginal Means, Aka Least-Squares Means." R. https://CRAN.R-project.org/package=emmeans.

[59] Kurc, S.A., and L.M. Benton. 2010. "Digital Image-Derived Greenness Links Deep Soil Moisture to Carbon Uptake in a Creosotebush-Dominated Shrubland." Journal of Arid Environments 74 (5): 585–94. https://doi.org/10.1016/j.jaridenv.2009.10.003.

[60] Munson, Seth M., and A. Lexine Long. 2017. "Climate Drives Shifts in Grass Reproductive Phenology across the Western USA." New Phytologist 213 (4): 1945–55. https://doi.org/10.1111/nph.14327.

[61] Reynolds, James F., Paul R. Kemp, Kiona Ogle, and Roberto J. Fernández. 2004. "Modifying the 'Pulse–Reserve' Paradigm for Deserts of North America: Precipitation Pulses, Soil Water, and Plant Responses." Oecologia 141 (2): 194–210. https://doi.org/10.1007/s00442-004-1524-4.

[62] Gremer, Jennifer R., John B. Bradford, Seth M. Munson, and Michael C. Duniway. 2015. "Desert Grassland Responses to Climate and Soil Moisture Suggest Divergent Vulnerabilities across the Southwestern United States." Global Change Biology 21 (11): 4049–62. https://doi.org/10.1111/gcb.13043.

[63] Bunting, Erin L., Seth M. Munson, and Miguel L. Villarreal. 2017. "Climate Legacy and Lag Effects on Dryland Plant Communities in the Southwestern U.S." Ecological Indicators 74 (March): 216–29. https://doi.org/10.1016/j.ecolind.2016.10.024.

[64] Yan, Dong, Xiaoyang Zhang, Shin Nagai, Yunyue Yu, Tomoko Akitsu, Kenlo Nishida Nasahara, Reiko Ide, and Takahisa Maeda. 2019. "Evaluating Land Surface Phenology from the Advanced Himawari Imager Using Observations from MODIS and the Phenological Eyes Network." International Journal of Applied Earth Observation and Geoinformation 79 (July): 71–83. https://doi.org/10.1016/j.jag.2019.02.011.

[65] Brown, Luke A., Booker O. Ogutu, and Jadunandan Dash. 2020. "Tracking Forest Biophysical Properties with Automated Digital Repeat Photography: A Fisheye Perspective Using Digital Hemispherical Photography from below the Canopy." Agricultural and Forest Meteorology 287 (June): 107944. https://doi.org/10.1016/j.agrformet.2020.107944.

[66] Filippa, Gianluca, Edoardo Cremonese, Mirco Migliavacca, Marta Galvagno, Oliver Sonnentag, Elyn Humphreys, Koen Hufkens, et al. 2018. "NDVI Derived from Near-Infrared-Enabled Digital Cameras: Applicability across Different Plant Functional Types." Agricultural and Forest Meteorology 249 (February): 275–85. https://doi.org/10.1016/j.agrformet.2017.11.003.

[67] Hufkens, Koen, Mark Friedl, Oliver Sonnentag, Bobby H. Braswell, Thomas Milliman, and Andrew D. Richardson. 2012. “Linking Near-Surface and Satellite Remote Sensing Measurements of Deciduous Broadleaf Forest Phenology.” Remote Sensing of Environment 117 (February): 307–21. https://doi.org/10.1016/j.rse.2011.10.006.

[68] Huete, A, K Didan, T Miura, E.P Rodriguez, X Gao, and L.G Ferreira. 2002. “Overview of the Radiometric and Biophysical Performance of the MODIS Vegetation Indices.” Remote Sensing of Environment 83 (1–2): 195–213. https://doi.org/10.1016/S0034-4257(02)00096-2.

[69] Paruelo, José M., and William K. Lauenroth. 1998. “Interannual Variability of NDVI and Its Relationship to Climate for North American Shrublands and Grasslands.” Journal of Biogeography 25 (4): 721–33. https://doi.org/10.1046/j.1365-2699.1998.2540721.x.

[70] Petrie, M. D., N. A. Brunsell, R. Vargas, S. L. Collins, L. B. Flanagan, N. P. Hanan, M. E. Litvak, and A. E. Suyker. 2016. “The Sensitivity of Carbon Exchanges in Great Plains Grasslands to Precipitation Variability.” Journal of Geophysical Research: Biogeosciences 121 (2): 280–94. https://doi.org/10.1002/2015JG003205.